JOURNAL of ELECTROCHEMICAL SCIENCE and TECHNOLOGY

RESEARCH ARTICLE

Clarification of Solid-State Synthesis Mechanism of Ni-Rich (Ni = 0.88) Layered Cathode Materials for Lithium-Ion Batteries

Hwasuk Nam | Keebum Hwang | Minki Oh | Youngmin Chi | Hyunchul Kang Songhun Yoon*

School of Integrative Engineering, Chung-Ang University, 221, Heuk-seok-Dong, Dongjak-Gu, Seoul 156-756, Republic of Korea

ABSTRACT

Owing to the widespread adoption of lithium-ion batteries in electric vehicles, energy storage systems, portable electronics, and various other applications, the demand for high-energy-density lithium-ion batteries with improved performance has increased dramatically. To address this critical need, this study investigates the solid-state synthesis mechanism of the Ni-rich LiNiCoMO (NCM) cathode material during calcination. $LiNi_{0.88}Co_{0.06}Mn_{0.06}O_2$ powders were prepared by first mixing $LiOH{\cdot}H_2O$ and $Ni_{0.88}Co_{0.06}Mn_{0.06}(OH)_2$. The mixture was then calcined for 0–15 h while gradually increasing the temperature from 225–700°C. The impact of calcination temperature on the structural and morphological changes was systematically analyzed via thermal, morphological, and crystal-structure analyses. The appropriate calcination temperature for acquiring the desired crystal structure was determined through weight changes during heating. The results revealed the initial formation of a rock-salt type of transition metal oxide phase at approximately 300°C, followed by lithium-ion diffusion into this structure, leading to a solid-solution phase at approximately 400°C. Subsequently, LiOH diffuses directly into the NCM powder at approximately 500°C through a solid-state reaction, initiating the formation of a layered phase. As the temperature rises to 700°C, this lithium-ion diffusion process further progresses, leading to a well-ordered layered structure, which is crucial for electrochemical performance. Increasing the dwell time at 700°C resulted in a stable cathode performance after 10 h. The study findings provide valuable insights into the structural optimization of NCM materials and contribute to the advancement of lithium-ion batteries.

KEYWORDS

Ni-rich NCM cathode material, Lithium-ion batteries, Calcination temperature, Solid-state reaction

CORRESPONDENCE
T: +82-2-820-5769
F: +82-2-814-2651
E: yoonshun@cau.ac.kr
https://doi.org/10.33961/jecst.2024.01151

VOLUME 16 ISSUE 2 MAY 2025

RECEIVED 31 October 2024 **ACCEPTED** 28 November 2024

INTRODUCTION

Lithium-ion batteries (LIBs) are the most suitable power sources for various portable electronic devices, energy-storage systems, and electric vehicles (EVs) owing to their high energy density, high operating voltage, and long cycle life [1,2]. In particular, global warming and carbon-neutrality policies are driving the electrification of transport systems to reduce global CO_2 emissions, further increasing the demand for environmentally sustainable technologies. Consequently, high-energy-density LIBs are necessary to meet the rapidly growing demand for EVs [3,4].

The cathode material plays a crucial role in determining the overall performance of LIBs. Many candidates are being explored for cathode materials, including $LiCoO_2$ (LCO), $LiNiO_2$ (LNO), $LiFePO_4$ (LFP), Li $(Ni_xCo_yAl_z)O_2$ (NCA), and Li $(Ni_xCo_yMn_z)O_2$ (NCM). Among these, layered lithium transition metal oxides, particularly Li $(Ni_xCo_yMn_z)O_2$, are promising for LIBs because of their high specific capacity, low toxicity, and low cost [5–8]. Moreover, Ni-rich LiNiCoMO (NCM) cathodes, which feature high energy density and good rate capability, are considered optimal for EV applications. However, the commercialization of these cathodes is challenging owing to thermal instability and poor cycle performance [9]. Therefore, several researchers and manufacturers are focusing on improving cathodes to meet the demands for higher energy density, thermal stability, and long cycle life.

The morphology and structure of the cathode material can significantly affect the cathode behavior, and the performance of NCM is dependent on its microstructure and crystal structure [10]. Therefore, understanding the structural changes that occur with temperature and time is essential for achieving the desired synthesis [11]. In this study, we systematically synthesized $LiNi_{0.88}Co_{0.06}Mn_{0.06}O_2$ cathode material at various calcination temperatures and durations to investigate the structural and morphological evolution as well as its impact on the electrochemical performance.

EXPERIMENTAL

Synthesis of cathode materials

The Ni–Co–$Mn(OH)_2$ precursor with an Ni:Co:Mn molar ratio of 0.88:0.06:0.06, synthesized via co-precipitation, was obtained from POSCO. This precursor, $Ni_{0.88}Co_{0.06}Mn_{0.06}(OH)_2$, was mixed with $LiOH{\cdot}H_2O$ (Li:TM = 1:1) and calcined under an O_2 atmosphere in a tube under the following conditions: temperatures of 225, 250, 275, 300, 400, 500, and 600°C for 0 h and 700°C for 0–15 h.

Material characterization

The crystal structure was analyzed via X-ray diffraction (XRD; New D8-Advance, Brooker-AXS with Cu Kα radiation) with a scan rate of 2.75°/min in the range of 10–90°. Particle surface morphology was observed via field emission scanning electron microscopy (FE-SEM, JEOL) at 5 kV. Energy-dispersive X-ray spectroscopy (EDS) was conducted at 20 kV using SIGMA 300 (Carl Zeiss) to qualitatively analyze the elemental distribution on the particle surface. Cross-sections of the particles were polished prior to the analysis.

Electrochemical performance evaluation

To evaluate the electrochemical performance, the cathode material was mixed with polyvinylidene fluoride (PVDF) binder and Super P conductive carbon black in a weight ratio of 94:3:3. The mixture was then dispersed in n-methylpyrrolidine (NMP) to form a slurry, which was then coated onto an Al foil. After drying in an oven at 120°C for 15 min, coin-type electrodes with a diameter of 10 mm (Ø10) were obtained through roll pressing and punching. These electrodes were then dried in a vacuum oven at 120°C for 12 h. Subsequently, they were sequentially assembled into 2032 coin-type half-cells with a Li-metal counter electrode. $LiPF_6$ (1 M), composed of ethylene carbonate and ethyl methyl carbonate (EC:EMC = 3:7 (volume ratio)), was used as the electrolyte. The electrochemical performance of the cell was evaluated by constant current cycling in the voltage range of 3.0–4.3 V vs. Li/Li^+ at room temperature.

RESULTS AND DISCUSSION

Thermogravimetric analysis (TGA)

TGA was conducted to observe the compositional changes in the Ni–Co–$Mn(OH)_2$ precursor and the Ni–

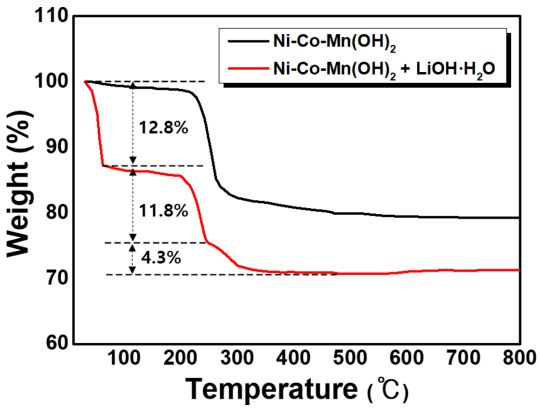

Fig. 1. TGA curve of the NCM under oxygen atmosphere at temperatures ranging from 35–800°C.

Co–Mn(OH)$_2$ mixed with LiOH·H$_2$O during calcination. The analysis was performed under flowing O_2 air at a heating rate of 2°C/min from 35–800°C as shown in Fig. 1. The TGA curve for the formation of Ni–Co–Mn cathode material exhibits three significant weight loss regions: 31–100, 200–250, and 250–500°C. The first weight loss (12.8%) can be attributed to the dehydration of LiOH·H$_2$O [12]. The second weight loss (11.8%) can be ascribed to the decomposition of Ni–Co–Mn(OH)$_2$ to (Ni–Co–Mn)O and H_2O. The weight loss (4.3%) is related to the reaction of (Ni–Co–Mn)O with the lithium source and the formation of lithiated nickel-cobalt-manganese oxide (Li(Ni–Co–Mn)O_2). By contrast, the TGA curve of the Ni–Co–Mn(OH)$_2$ precursor shows a sharp weight decrease only around 250°C, indicating that a calcination temperature above 500°C is required to obtain a layered structure of the NCM cathode material.

XRD

XRD analysis was performed to trace the reaction pathway and synthesis mechanism of the $Li(Ni_{0.88}Co_{0.06}Mn_{0.06})O_2$ cathode material during calcination. Fig. 2 shows the XRD patterns of the NCM compound synthesized at temperatures ranging from 225–700°C. The synthesized samples were designated based on the temperature; for example, NCM-700 indicates an NCM powder calcined at 700°C. When only the precursor was mixed with the lithium source, the XRD pattern showed peaks corresponding to M(OH)$_2$ (denoted as M = Ni–Co–Mn) and LiOH·H$_2$O [13]. The LiOH peak was attributed to the dehydration of LiOH·H$_2$O synthesized at 225–250°C [14]. At 300°C, the peak of the M(OH)$_2$ precursor disappeared and the MO peak increased. Around 400°C, the LiOH peaks significantly diminished owing to Li diffusion into the MO structure through a solid-state reaction, causing a decrease in lattice size and transformation to the $Li_xM_{1-x}O$ phase. At 500°C, only the MO peak remained and gradually shifted to a higher angle. However, the XRD patterns of the powder synthesized at 500°C for 5 h revealed peaks corresponding to $LiMO_2$, indicating a solid-state reaction with the lithium source. No further phase changes were observed, suggesting that a calcination temperature of at least 500°C with an appropriate dwell time is sufficient to obtain the layered crystal structure. Increasing the temperature to 700°C resulted in sharper peaks than those of NCM-600, indicating crystal growth of the $LiMO_2$ phase. Additionally, all diffraction peaks were indexed to the α-$NaFeO_2$ structure with a hexagonal-type of R-3m space group, indicating no crystalline impurities [15]. Sintering NCM-700 for 0, 5, and 15 h further increased the peak, leading to a clear splitting of (108)/(110) peaks, thereby confirming the formation of a well-ordered layered structure in the $LiMO_2$ cathode material [16]. Additionally, the values of I(003)/I(104) corresponding to the calcination times of 0, 5, and 15 h are 1.28, 1.88, and 1.91, respectively. This observation highlights the importance of a sufficient temperature and retention time to form the layered structure of the Ni-rich NCM cathode material. Furthermore, the (104) peak shifted to a higher angle and the (003) peak appeared (up to 500°C), demonstrating the formation of the R-3m layered phase [17].

SEM/EDS

Fig. 3–7 show the morphologies and surface chemistries of the powders calcined at 225, 300, 400, and 500°C for 0 h and 700°C for 15 h, as analyzed via SEM and EDS mapping. In the powder prepared at 225°C

(Fig. 3), a dark region circled in yellow was identified in the SEM image. EDS mapping showed that these regions lacked Ni, Co, and Mn signals. Moreover, numerous non-spherical, nano-sized, and irregular particles were observed, as depicted in Fig. S1. These findings suggest that the lithium source did not react with the NCM hydroxide precursor and remained on the particle surface.

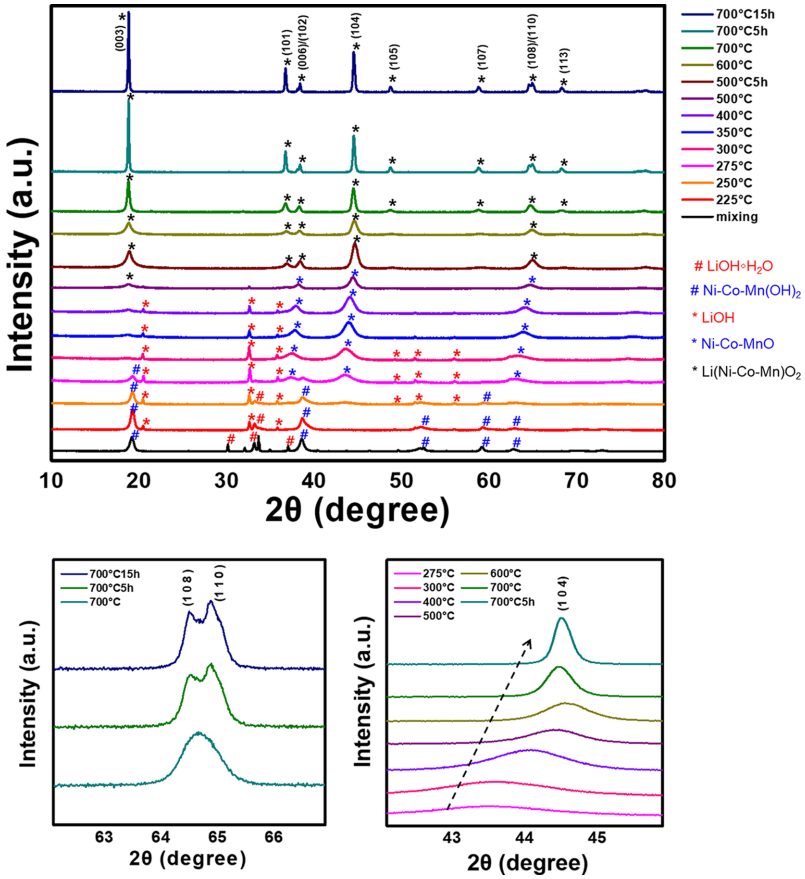

Fig. 2. XRD patterns of the NCM powders calcined at different temperatures and magnification of (104) and (108)/(110) peaks.

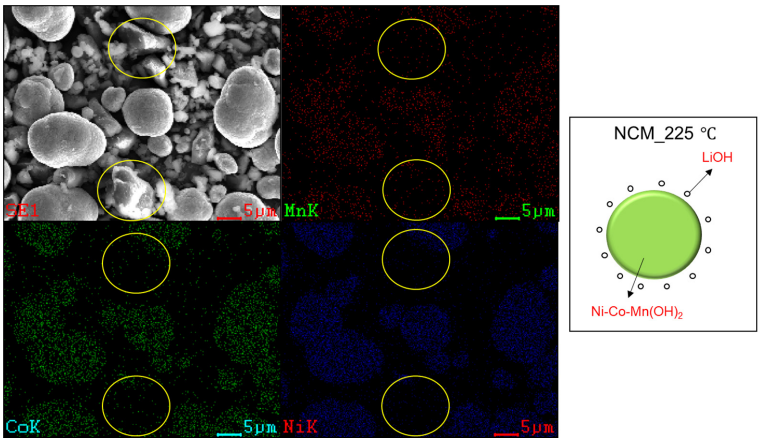

Fig. 3. SEM and EDS mapping images of the NCM samples calcined at 225°C for 0 h.

Fig. 4 indicates that dark regions are present even in the sample calcined at 300°C, implying that although the precursor reacted with oxygen to form the (Ni–Co–Mn)O phase, the LiOH particles still remained on the surface.

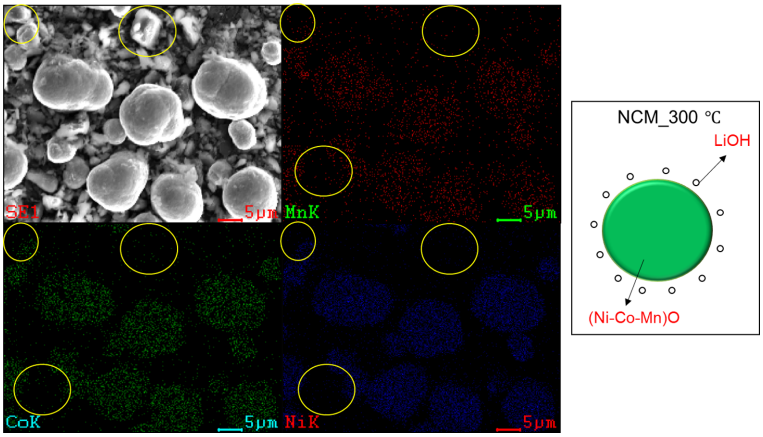

Fig. 4. SEM and EDS mapping images of the NCM samples calcined at 300°C for 0 h.

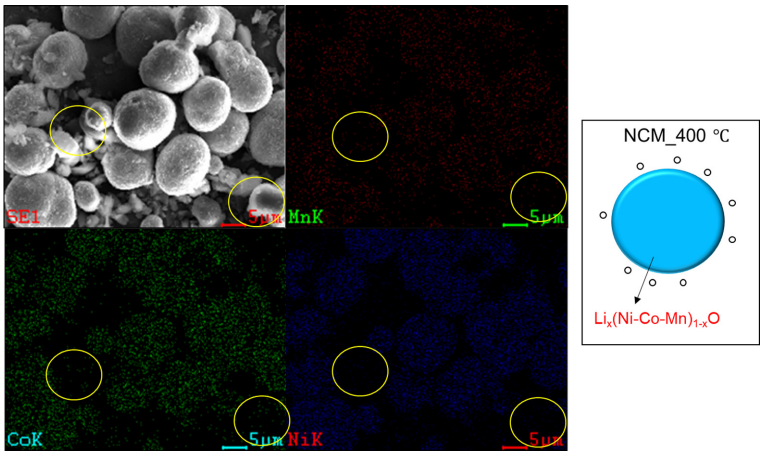

Fig. 5. SEM and EDS mapping images of the NCM samples calcined at 350°C for 0 h.

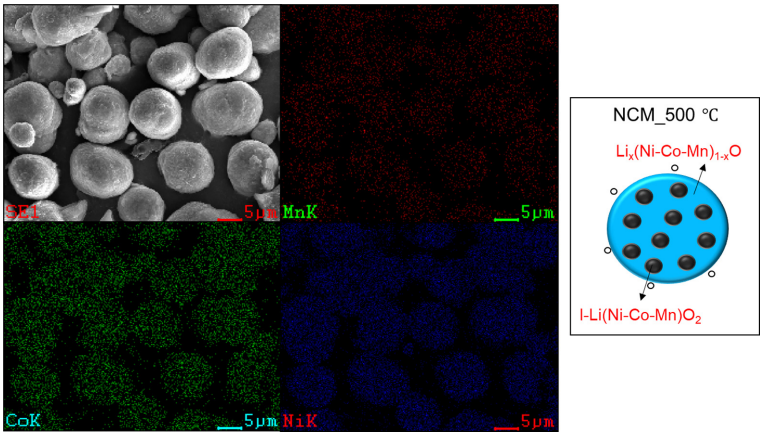

Fig. 6. SEM and EDS mapping images of the NCM samples calcined at 500°C for 0 h.

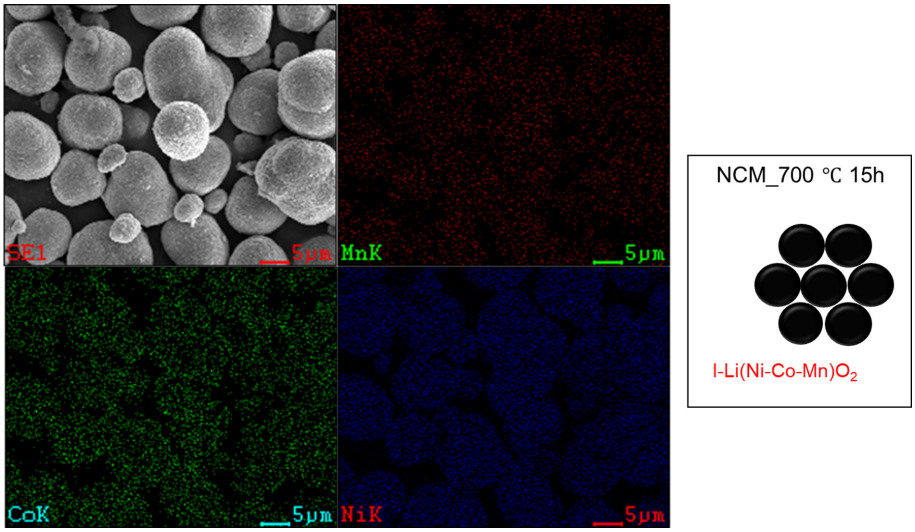

Fig. 7. SEM and EDS mapping images of the NCM samples calcined at 700°C for 15 h.

The powder synthesized at 400°C also shows the same LiOH particles (Fig. 5); however, a new rod-shaped phase that was not observed at lower temperatures was detected as shown in Fig. S3. This suggests that some LiOH started reacting with (Ni–Co–Mn)O to form a lithiated NCM ($Li_x(Ni–Co–Mn)_{1–x}O$) phase through a solid-state reaction. Increasing the temperature to 500°C eliminated the dark regions (Fig. 6), probably because the melting point of LiOH is approximately 462°C. This allowed some lithium to directly diffuse into the NCM structure, leading to complete synthesis and gradual transformation into a layered phase, consistent with the XRD results. Additionally, most secondary particles became spherical after calcination (Fig. S4)

Thus, it was confirmed that increasing the temperature and time (700°C for 15 h) noticeably reduced the submicron particles compared to that at low temperatures, and the secondary particles were composed of primary particles with a layered phase (Fig. 7 and S5).

Proposed synthesis mechanism

Fig. 8 illustrates the synthesis mechanism of Ni-rich NCM cathode material at various calcination temperatures, highlighting the key structural changes. The overall reaction can be summarized as follows:

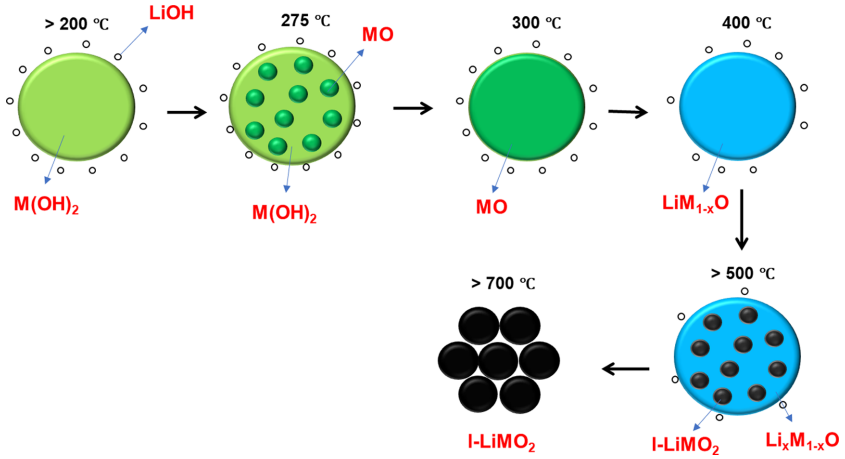

Fig. 8. Schematic of the synthesis mechanism for the reaction of Ni-rich NCM cathode material calcined at different temperatures (M = $Ni_{0.88}Co_{0.06}Mn_{0.06}$).

1. At 100°C, lithium hydroxide monohydrate undergoes dehydration:
   $LiOH{\cdot}H_2O \rightarrow LiOH + H_2O$ (31–100°C)

2. At approximately 275°C, $M(OH)_2$ undergoes dehydration, producing an MO phase:
   $M(OH)_2 \rightarrow MO + H_2O$ (200–275°C)

3. As the melting point of LiOH is approximately 462°C, LiOH directly reacts with MO in the solid phase to form a $Li_xNi_{1-x}O$ phase between 275 and 470°C:
   $MO + LiOH + O_2 \rightarrow Li_xM_{1-x}O + H_2O$ (275–470°C)

4. Above 470°C, the produced $Li_xM_{1-x}O$ reacts completely with LiOH in a solid-state reaction to form a $LiMO_2$ layered phase:
   $Li_xM_{1-x}O + LiOH + O_2 \rightarrow LiMO_2$ (>470°C)

Electrochemical performance

To investigate the effect of different calcination holding times on the electrochemical performance of the $LiNi_{0.88}Co_{0.06}Mn_{0.06}O_2$ cathode, 2023 coin-type half-cells with Li foil were assembled as the counter electrode. The cathode materials were initially calcined at 480°C for 2 h and then at 700°C for 5, 10, and 15 h, as shown in Fig. 8. Fig. 9a–c shows the charge–discharge curves in a voltage range of 3.0–4.3 V at 1 C for the 1st, 25th, and 50th cycles. Evidently, all samples exhibit a voltage plateau near 4.08 V; however, for the sample calcined for 15 h, it disappears near 3.5 V after 50 cycles. According to the results presented in Table S1, residual Li compounds decrease as the calcination time increases. The initial discharge capacities of the samples calcined for 5, 10, and 15 h are 193.54, 202.98, and 201.47 mAh/g, respectively. The sample calcined at 700°C for 15 h exhibits the highest capacity retention, which is attributed to a reduction in residual lithium and increased particle size with longer holding times.

Fig. 10 shows the rate capability and c-rate efficiency at various current densities (0.1, 0.2, 0.5, 1, 2, and 4 C) and in the voltage range of 3.0–4.3 V. All samples demonstrate similar specific capacities and c-rate efficiencies at all current densities. However, the sample calcined at 700°C for 5 h exhibits the highest rate efficiency, primarily owing to its smaller particle size than the other samples. Typically, small particle sizes in NCM cathode materials enhance their power characteristics.

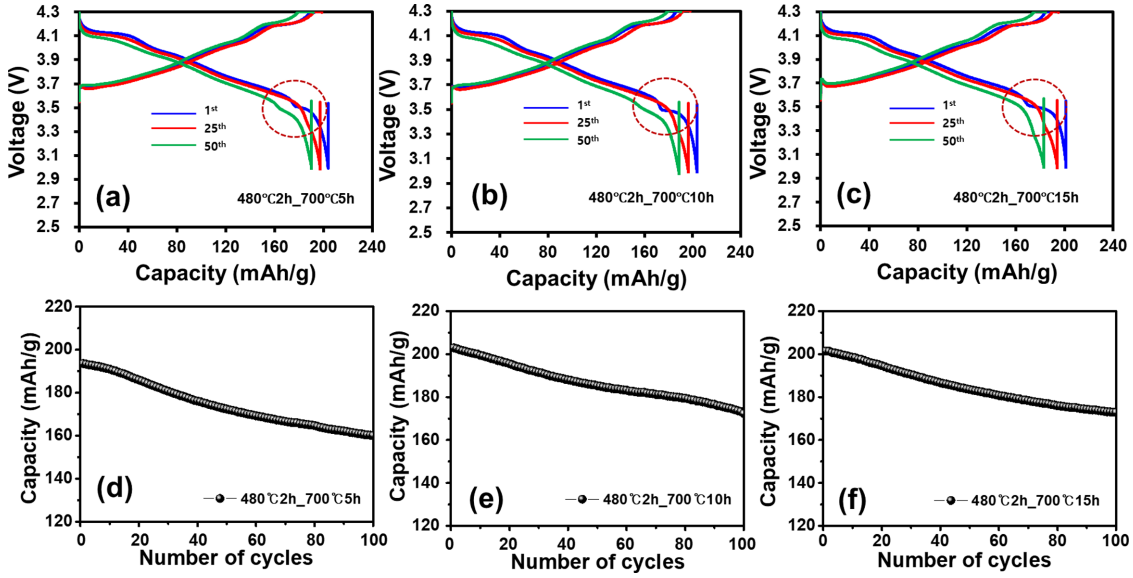

Fig. 9. Selected voltage profiles for the 1st, 20th, and 50th cycles and cycling performance between 3.0 and 4.3 V of $LiNi_{0.88}Co_{0.06}Mn_{0.06}O_2$ cathode materials calcined at 700°C for (a, d) 5, (b, e) 10, and (c, f) 15 h after preheating at 480°C for 2 h.

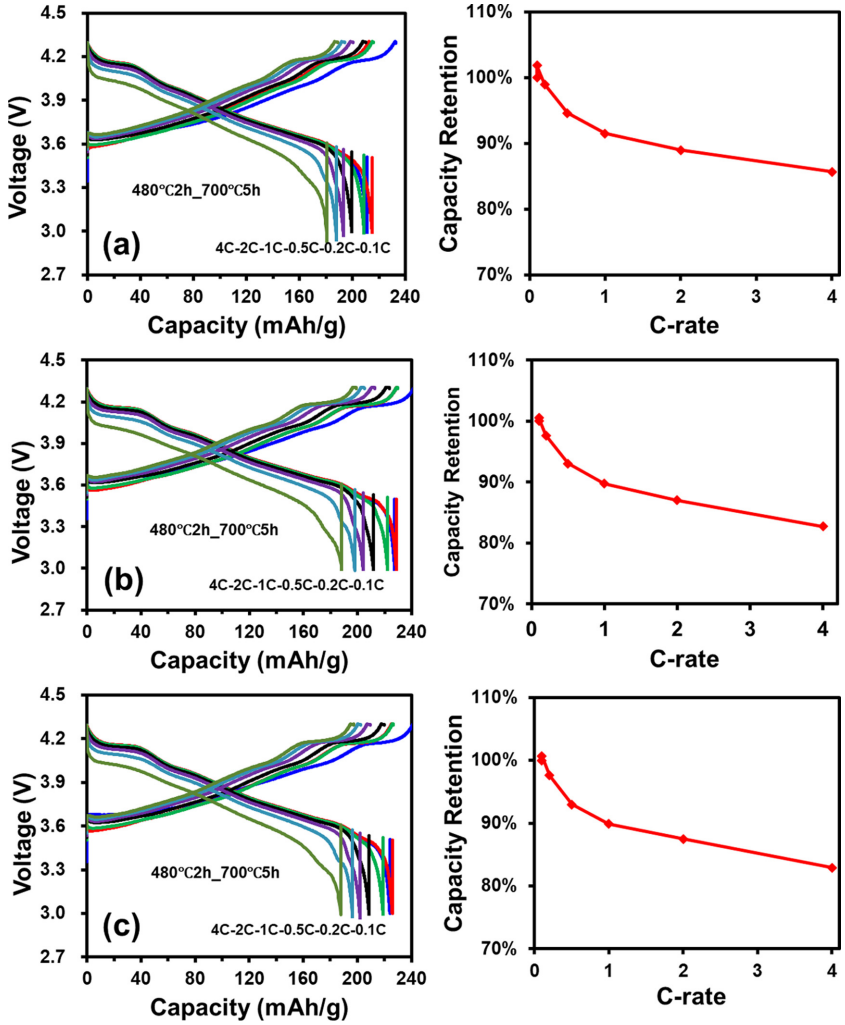

Fig. 10. Rate capability and c-rate efficiency in the voltage range of 3.0–4.3 V and at various current densities (0.1, 0.2, 0.5, 1, 2, and 4C) of the $LiNi_{0.88}Co_{0.06}Mn_{0.06}O_2$ cathode materials calcined at 700°C for (a) 5, (b) 10, and (c) 15 h after preheating at 480°C for 2 h.

CONCLUSIONS

In this study, $Li(Ni_{0.88}Co_{0.06}Mn_{0.06})O_2$ powder was synthesized via high-temperature calcination, with the aim of investigating the detailed synthesis mechanism of the reaction between lithium salt and Ni–Co–$Mn(OH)_2$ at gradually increasing calcination temperatures. The structural evolution of the cathode material with temperature was analyzed to determine the formation of a layered structure. At 100°C, $LiOH{\cdot}H_2O$ underwent dehydration, which was followed by the dehydration of $M(OH)_2$ at approximately 275°C to form an MO phase. As the melting point of LiOH is approximately 462°C, it reacted with MO in the solid phase to form the $Li_xM_{1-x}O$ phase. Subsequently, $Li_xM_{1-x}O$ further reacted with LiOH in a solid-state reaction above 500°C to form a layered $LiMO_2$ structure. The results indicate that the structural changes during the NCM synthesis significantly influence the conductivity, thermal stability, and ion mobility of the cathode material. Specifically, the formation of a layered structure is crucial for achieving high energy density and rate capability. This study provides valuable insights into the structural optimization of NCM materials, and thereby contributes to the commercialization of LIBs.

ACKNOWLEDGEMENTS

This research was supported by the Chung-Ang University Graduate Research Scholarship in 2023.

This research was supported by Basic Science Research Program through the National Research Foundation of Korea (NRF) funded by the Ministry of Education (RS-2023-00255695).

REFERENCES

[1] G. Ko, S. Jeong, S. Park, J. Lee, S. Kim, Y. Shin, W. Kim, and K. Kwon, Energy Storage Mater., 2023, 60, 102840.

[2] J. Yan, H. Huang, J. Tong, W. Li, X. Liu, H. Zhang, H. Huang, and W. Zhou, Interdiscip. Mater., 2022, 1(3), 330–353.

[3] J. Yang, X. Liang, H.-H. Ryu, C. S. Yoon, and Y.-K. Sun, Energy Storage Mater., 2023, 63, 102969.

[4] M. Su, Y. Chen, Y. Song, A. Dou, J. Wang, G. Yan, Y. Zhou, Z. Wang, and Y. Liu, Chem. Eng. J., 2023, 477, 147202.

[5] Y. Liu, T. Zeng, G. Li, T. Wan, M. Li, X. Zhang, M. Li, M. Su, A. Dou, W. Zeng, Y. Zhou, R. Guo, and D. Chu, Energy Storage Mater., 2022, 52, 534–546.

[6] Y.-H. Chen, J. Zhang, Y. Li, Y.-F. Zhang, S.-P. Huang, W. Lin, and W.-K. Chen, Phys. Chem. Chem. Phys., 2021, 23, 11528–11537.

[7] M. Chu, Z. Huang, T. Zhang, R. Wang, T. Shao, C. Wang, W. Zhu, L. He, J. Chen, W. Zhao, and Y. Xiao, ACS Appl. Mater. Interfaces, 2021, 13(17), 19950–19958.

[8] C. Wendt, P. Niehoff, M. Winter, and F. M. Schappacher, J. Power Sources, 2018, 391, 80–85.

[9] G. W. Nam, N.-Y. Park, K.-J. Park, J. Yang, J. Liu, C. S. Yoon, and Y.-K. Sun, ACS Energy Lett., 2019, 4(12), 2995–3001.

[10] A. Habibi, M. Jalaly, R. Rahmanifard, and M. Ghorbanzadeh, New J. Chem., 2018, 42(23), 19026–19033.

[11] J. A. A. Abdullah, M. Jiménez-Rosado, A. Guerrero, and A. Romero, Materials, 2023, 16(5), 1798.

[12] M. Kubota, S. Matsumoto, H. Matsuda, H. Y. Huang, Z. H. He, and X. Yang, Adv. Mater. Res., 2014, 953–954, 757–760.

[13] S.-J. Lee and J.-T. Son, J. Korean Phys. Soc., 2021, 79(1), 1–4.

[14] C. M. Burke, R. Black, I. R. Kochetkov, V. Giordani, D. Addison, L. F. Nazar, and B. D. McCloskey, ACS Energy Lett., 2016, 1(4), 747–756.

[15] G. Li, L. Qi, P. Xiao, Y. Yu, X. Chen, and W. Yang, Electrochim. Acta, 2018, 270, 319–329.

[16] Y. Zhang, W. Zhang, S. Shen, X. Yan, R. Wu, A. Wu, C. Lastoskie, and J. Zhang, ACS Omega, 2017, 2(11), 7593–7599.

[17] D. Wang, X. Zhang, G. Zhong, Y. Li, C. Hong, K. Dong, C. Chen, and Y. Yang, J. Power Sources, 2022, 529, 231258.